

Recycled graphite for more sustainable lithium-ion batteries

Mayokun Olutogun^{1,2}  | Anna Vanderbruggen³  | Christoph Frey⁴ |
Martin Rudolph³  | Dominic Bresser^{1,2}  | Stefano Passerini^{1,2,5} 

¹Helmholtz Institute Ulm (HIU), Ulm, Germany

²Karlsruhe Institute of Technology (KIT), Karlsruhe, Germany

³Helmholtz Zentrum Dresden-Rossendorf (HZDR), Helmholtz Institute Freiberg for Resource Technology (HIF), Freiberg, Germany

⁴ProGraphite GmbH, Untergriesbach, Germany

⁵Chemistry Department, Sapienza University of Rome, Rome, Italy

Correspondence

Dominic Bresser, Helmholtz Institute Ulm (HIU), 89081 Ulm, Germany.
Email: dominic.bresser@kit.edu

Funding information

Bundesministerium für Bildung und Forschung, Grant/Award Numbers: 03XP0138C, 03XP0306C

Abstract

The demand for lithium-ion batteries (LIBs) is driven largely by their use in electric vehicles, which is projected to increase dramatically in the future. This great success, however, urgently calls for the efficient recycling of LIBs at the end of their life. Herein, we describe a froth flotation-based process to recycle graphite—the predominant active material for the negative electrode—from spent LIBs and investigate its reuse in newly assembled LIBs. It has been found that the structure and morphology of the recycled graphite are essentially unchanged compared to pristine commercial anode-grade graphite, and despite some minor impurities from the recycling process, the recycled graphite provides a remarkable reversible specific capacity of more than 350 mAh g⁻¹. Even more importantly, newly assembled graphite||NMC₅₃₂ cells show excellent cycling stability with a capacity retention of 80% after 1000 cycles, that is, comparable to the performance of reference full cells comprising pristine commercial graphite.

KEYWORDS

anode, graphite, lithium-ion battery, recycling, sustainability

1 | INTRODUCTION

Lithium-ion batteries (LIBs) are ubiquitous in our everyday life, powering our power tools, mobile phones, laptops, and other electronic devices—and increasingly also (hybrid) electric vehicles.^{1–3} The anticipated, essentially exponential increase in LIB sales, however, raises increasing concerns about their environmental impact and the availability of resources. The efficient recycling of LIBs at their end of life is thus essential for addressing these concerns.^{3,4} The current and emerging recycling technologies for LIBs typically focus on the recovery of components that have high economic value, such as Co,

Ni, Cu, and, more recently, Li.⁵ Most of these recycling technologies use the black mass (a mixture of anode and cathode active material particles) resulting from the pretreatment as a starting point for the further chemical processing to recover these valuable metals.⁶ Commonly, this black mass is usually not further sorted and is directly fed into the pyro- and/or hydrometallurgical processes to extract the metals from the cathode—at the expense of the complete loss of the graphite active material. At the same time, the presence of graphite in the black mass results in a higher water and reagent consumption and challenges in the dewatering stage,^{7–9} thus rendering the removal of the graphite phase before

This is an open access article under the terms of the [Creative Commons Attribution](https://creativecommons.org/licenses/by/4.0/) License, which permits use, distribution and reproduction in any medium, provided the original work is properly cited.

© 2024 The Authors. *Carbon Energy* published by Wenzhou University and John Wiley & Sons Australia, Ltd.

the further recycling of the metals highly desirable. Accordingly, an initial preconcentration of graphite using the froth flotation process to reduce its amount in the black mass before further processing and metal recycling has recently gained attention.^{10–14} This procedure advantageously results in higher yields of metallic species during the subsequent hydrometallurgical treatment. Nonetheless, the recovered graphite from spent commercial LIBs has not been studied for reuse in new LIBs so far.

To meet the revised Battery Directive, however, which includes an increase of the minimum recycling efficiency of 50% (wt/wt) (Directive 2006/66/EC) to 70% (wt/wt) by 2030, more efficient recycling strategies are required.¹⁵ To reach such ambitious levels, graphite must also be recycled, as it represents up to 25% of the total mass of LIBs and will remain an essential component of LIBs in the near to midterm future.¹⁶ Properly designed processes for the recovery of graphite from LIBs would also result in a diversification of the graphite supply, which is presently dominated by China with about 64% of the flake graphite global production and almost 90% of the spherical anode grade graphite used in LIBs.¹⁷ As a result, other countries are actively searching for strategies to develop their own graphite supply chain for battery production.

Herein, we report a froth flotation-based graphite recycling process from spent LIBs, followed by a comprehensive characterization of the recycled active material and its reuse in graphite||NMC₅₃₂ lithium-ion cells. The results underline the great potential of such reused graphite, providing comparable performance as pristine commercial graphite in terms of both reversible capacity and long-term cycling stability.

2 | EXPERIMENTAL SECTION

2.1 | The recycling process

A mixture of spent LIBs from portable electronic devices such as laptops and power tools with Li[Ni_{1-x-y}Mn_xCo_y]O₂ (NMC) and LiCoO₂ (LCO) cathode active materials was vacuum pyrolyzed (500°C–600°C) and crushed by an industrial scale operator, that is, Accurec Recycling GmbH (Germany). The resulting black mass was sieved to separate the differently sized fractions. The fraction below 100 µm was used as a flotation feed. The sieved particles were dispersed in tap water with a solid ratio of 50% (wt/wt) and subjected to a 10 min stirring at 16,000 rpm using an Ultra Turrax high shear mixer (IKA, dispersing tool: S25N-25F), as described in detail in a previous study.¹⁸ This pretreatment, referred to as

attrition, refreshes the particle surfaces by removing part of the residual binder and increases the wetting and dispersion of the particles in water. The froth flotation stage was conducted using a mechanically agitated OUTOTEC GTK lab cell with a 4 L cell laboratory flotation machine, an impeller speed of 1000 rpm, and an airflow rate of 7 L min⁻¹. Two reagents were used for the flotation: the collector was EscaldTM 110 from ExxonMobil (hydrocarbon fluid, product no. 20171206; concentration of 500 g t⁻¹, conditioned for 3 min), which enhances the graphite hydrophobicity. As the frothier, methyl isobutyl carbinol supplied by Alfa Aesar (99%, Product No. A13435; concentration of 150 g t⁻¹, conditioned for 1 min) was used. After flotation, 40% (wt/wt) of the flotation feed was collected in the froth phase with a grade of 85.2% carbon, corresponding to a recovery of 93.2% of the graphite from the spent LIBs. Chemical purification of the flotation product was conducted to remove the fine particles of lithium transition metal oxides, resulting in a very high purity of the recycled graphite with only about 0.8% metallic and sulfidic impurities. The sample material was sent to EcoGraf and treated using the EcoGraf purification process to remove the impurities. For this purpose, the material was intensively mixed with caustic soda before it was heated at temperatures of around 500°C. The water content of the caustic soda was evaporated and a cake was formed, which was first washed in a water bath, with the individual particles detaching from one another and being present as a dispersion. After filtering off, the aqueous dispersion was mixed with diluted sulfuric acid, and at moderate temperatures, the impurities associated with the sodium were dissolved by the acid and turned into a liquid state. After the reaction time had elapsed, the remaining graphite was filtered and then intensively washed until a neutral pH value was achieved.

2.2 | Physicochemical characterization

The morphology of the recycled graphite material was investigated using scanning electron microscopy (SEM; Zeiss Crossbeam 340 field-emission electron microscope). Energy-dispersive X-ray spectroscopy (EDX; Oxford Instruments X-Max Xtreme) was used to analyze the surface composition of the recycled graphite powder. Powder X-ray diffraction (XRD) was performed to investigate the crystal structure of the recycled graphite material, using a Bruker D8 Advance (Cu-K_{α1} radiation, λ = 0.154 nm) equipped with a graphite monochromator. The diffractograms were recorded within the 2θ range between 20° and 80° with a 0.02° step size and 9 s counting time per step. The specific surface area was determined via

nitrogen adsorption using an Autosorb-iQ (Quantachrome) following the Brunauer–Emmett–Teller method. Raman spectra were recorded in the backscattering configuration with a microspectrometer (Renishaw) in conjunction with an InVia confocal microscope. The experiments were carried out using an excitation wavelength of 532 nm (2.31 eV). Thermogravimetric analysis coupled with mass spectrometry (TGA-MS) was conducted by means of a TG 209 F1 (NETZSCH) and QMS 403 D (Aeolos), respectively. For these experiments, the recycled graphite samples were weighed and placed in open high-temperature Al₂O₃ pans. Initially, a thermal equilibration step at 30°C for 30 min was applied. Thereafter, the samples were heated to 1000°C at a rate of 5 K min⁻¹ under either oxygen or helium atmosphere. X-ray photoelectron spectroscopy (XPS) was conducted using a PHI 5800 Multi-Technique ESCA system (Physical Electronics) with monochromatic Al-K α radiation (1486.6 eV). The detection angle was 45° and pass energies of 93.9 and 29.35 eV were used for both the survey and the detailed spectra at the analyzer. Charging effects at the surface were compensated with the use of low-energy electrons from a flood gun. The binding energies of all spectra were calibrated to the main C (1s) peak at 284.8 eV of adventitious carbon. The results were analyzed using the CasaXPS software. Inductively coupled plasma optical emission spectroscopy (ICP-OES) was carried out using a Spectro Acros-SOP system. For the analysis, 20 mg of each sample was dissolved in 25 mL aqua regia (HNO₃:HCl in a 3:1 ratio). Subsequently, the mixture was filtered, and the resulting solution was diluted with deionized water, depending on the detection and calibration regime of the element of interest. Each experiment was repeated at least thrice for the sake of reproducibility and the standard deviation was calculated.

2.3 | Electrode preparation

Recycled graphite, as the active material for the negative electrode, was mixed with conductive carbon (C-ENERGY, Super C45; Imerys), sodium carboxymethyl cellulose (CMC; Dow Wolff Cellulosics), and styrene-butadiene rubber (SBR; Zeon) in deionized water to form a homogenous paste. The resulting slurry was cast on copper foil using a laboratory-scale doctor blade. The wet electrodes were dried at 80°C under an ambient atmosphere. The final composition of the electrodes, expressed as the weight ratio of the active material, conductive agent, CMC, and SBR, was 96:1:1:2. Subsequently, disc-shaped electrodes with a diameter of 12 mm were punched and dried at 110°C under vacuum for 12 h. The electrode active mass loading was either about 3.20 mg cm⁻², corresponding to an initial and reversible

areal capacity of 1.30 and 1.07 mAh cm⁻², respectively, or 6.24 mg cm⁻², corresponding to an initial and reversible areal capacity of 2.53 and 2.09 mAh cm⁻², respectively. The graphite electrodes were pressed at 0.5 t for 10 s, resulting in an electrode coating density of about 1.3 g cm⁻³ and an estimated porosity of about 34%. Following the same recipe and processing, also electrodes based on commercial graphite (SLP30; Imerys) were prepared for a direct comparison.

Li[Ni_{0.5}Mn_{0.3}Co_{0.2}]O₂ (NMC₅₃₂) powder (TODA, average particle size of 10 μ m) was used as the active material for the positive electrode. A homogeneous slurry was prepared by mixing the active material, conductive carbon (C-ENERGY Super C65; Imerys), and polyvinylidene fluoride (PVdF 6020; Solvay) in *N*-methyl-2-pyrrolidone (NMP; Aldrich). The resulting slurry was cast on aluminum foil and dried at 60°C under ambient atmosphere to remove NMP. The final composition of the NMC₅₃₂ electrodes, expressed as weight ratio of the active material, conductive agent, and PVdF, was 92:4:4. Thereafter, disc-shaped electrodes with a diameter of 12 mm were punched and dried under vacuum at 110°C for 12 h. The electrode active mass loading was either about 6.40 mg cm⁻², corresponding to an initial and reversible areal capacity of 1.18 and 1.08 mAh cm⁻², respectively, or 12.47 mg cm⁻², corresponding to an initial and reversible areal capacity of 2.30 and 2.10 mAh cm⁻², respectively. Subsequently, the NMC₅₃₂ electrodes were pressed at 10 t for 10 s, resulting in an electrode density of about 2.7 g cm⁻³.

2.4 | Electrochemical characterization

The electrochemical tests in half-cells were conducted at room temperature (20°C) using three-electrode Swagelok™-type cells. Lithium-metal foil (Honjo, lithium battery grade) was used for the counter and reference electrodes. The half-cells were assembled in an argon-filled glove box (MBraun, O₂ < 0.1 ppm and H₂O < 0.1 ppm). Whatman GF/D glass fiber sheets were used as the separator. As the electrolyte, 120 μ L of the 1 M LiPF₆ solution in ethylene carbonate and diethyl carbonate (EC:DEC = 1:1 vol/vol), comprising 2 wt% vinylene carbonate (VC) and 10 wt% fluoroethylene carbonate (FEC), supplied by Solvionic, was used. FEC was added to reduce the side reactions occurring at the lithium-metal counter electrode for the half-cell tests. Cyclic voltammetry (CV) was conducted utilizing a VMP3 potentiostat (BioLogic). The sweep rate was set to 0.1 mV s⁻¹, and the reversing potentials were set to 0.01 and 1.0 V versus Li⁺/Li.

The galvanostatic full-cell tests were carried out in Swagelok™-type three-electrode cells with lithium foil

(battery grade; Honjo) as the reference electrode to selectively evaluate the potential profiles of the anode and cathode. For the long-term cycling tests, CR2032 (Hohsen) coin cells were used. The graphite anodes had a reversible areal capacity of about 1.0 and 2.0 mAh cm⁻² and were matched with suitable NMC₅₃₂ cathodes to obtain an N:P ratio of about 1.1. The polyethylene-based separators (10 μm; Asahi) were drenched in both cases with 80 μL of the electrolyte, that is, 1 M LiPF₆ in EC:DMC (1:1) vol/vol + 2 wt% VC. Both the half-cell and full-cell cycling tests were performed in climatic chambers (Binder) at a temperature of 20 ± 1°C. The cells were allowed to rest for 24 h before the measurements were conducted using a Maccor Series 4300 Battery tester. The cycling procedure for the full cells comprises a constant current/constant voltage (CC/CV) step during charge followed by a CC discharge with 4.3 and 2.5 V as the upper and lower cutoff voltage. The first cycle was performed at C/20 and the subsequent cycles were performed at C/2. A discharge/charge rate of

1 C corresponds to a specific current of 350 mA g⁻¹ for the graphite half-cell tests and to 170 mA g⁻¹ for the full-cell tests.

3 | RESULTS AND DISCUSSION

3.1 | The recycling process

The froth flotation-based recycling process for spent LIBs with a particular focus on the graphite anode is depicted in Figure 1. At each step, the carbon grade of the resulting product was determined, along with an estimation of the overall recovery rate after the complete recycling process. The black mass used as the feed for this recycling process, provided by Accurec Recycling GmbH (Germany), was obtained from spent LIBs with NMC and LCO-positive electrodes. The spent batteries initially underwent a vacuum thermal treatment at

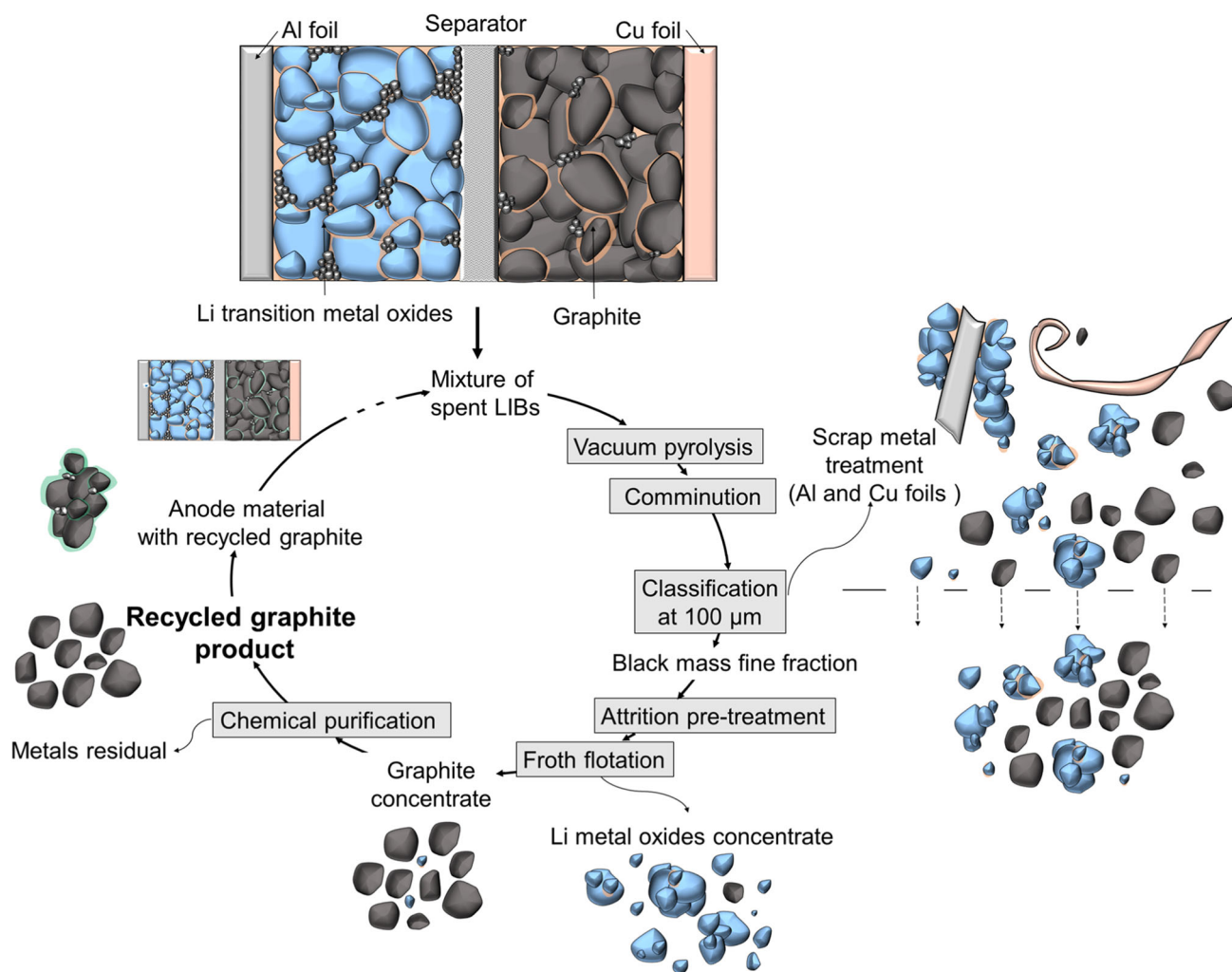


FIGURE 1 Schematic illustration of the lithium-ion battery recycling process with a particular focus on closing the loop of graphite from the anode.

500°C–600°C (vacuum pyrolysis) to deactivate them and enable safer mechanical processing. The thus treated and subsequently crushed product was then size classified by sieving. The fractions below 1 mm of this industrial black mass were characterized using automated mineralogy analysis as described by Vanderbruggen et al.¹⁹ This analysis provides valuable information on the LIB components such as the elemental composition, the particle morphology, and the degree of liberation. In the present case, the graphite particles were well liberated from the copper current collector, as about 98% of the graphite particles in the 1 mm fraction ended up in the fraction below 100 μm . This assumption appears reasonable, given that most of the polymer binder is removed during the pyrolysis step, resulting in the high degree of graphite particle liberation observed. The fraction below 100 μm was obtained by sieving and used as a flotation feed. The fine particles were dispersed in tap water with a solid ratio of 50% (wt/wt) by high-shear mixing.¹⁸ This pretreatment, referred to as attritioning, refreshes and reactivates the particles' surfaces by removing part of the residual binder and, thus, increases the wetting and dispersion of the graphite particles in water. After the froth flotation step, 40% (wt/wt) of the flotation feed was collected in the froth phase with a carbon grade of 85.2%, which translates into a recovery rate of 93.2% of the overall graphite content from the spent LIBs. Subsequently, a chemical purification (developed by EcoGraf) of the flotation product was conducted to remove any residual cathode elements, yielding recycled graphite with a very high purity (further specified below) and only about 0.8% metallic and sulfidic impurities.

3.2 | Physicochemical characterization of the recycled graphite

Figure 2A–D shows SEM images of the recycled graphite material (additional images are provided in Figure S1). Generally, a mixture of potato-shaped and flake-like particles with a size of several tens of micrometers was observed, along with some smaller particles of a less homogeneous morphology. The latter potentially result from some fracturing of the characteristic potato-shaped or flake-like graphite particles, which might have happened during the original electrode fabrication or the shredding and/or attrition step during the recycling process. Figure 2D presents a close-up of one of the potato-shaped particles, revealing that the surface of the graphite particles is partially covered with smaller particles of a few 100 nm, which results in a specific surface area of about 6.9 m^2g^{-1} . EDX mapping shows that these smaller particles are essentially composed of

carbon (and to a minor extent of oxygen), suggesting that this might be residual conductive carbon black and other carbonaceous species resulting from the electrode and/or the recycling process. This is in line with the results of the TGA-MS performed under an oxygen atmosphere (Figure S2A), which shows a mass loss of essentially 100%, accompanied by CO_2 release. A minor fraction of about 4.3% is even released under a helium atmosphere (Figure S2B), indicating that part of these species (potentially organic components of the solid electrolyte interphase, which have not been washed away during the recycling process, or other carbon species that are reacting with the remaining oxygen) are turning gaseous even in the absence of oxygen. The TGA-MS data are in good agreement with the results obtained by XPS (Table S1) and ICP-OES (Table S2) to detect potential impurities at the surface and in the bulk phase, respectively.

The XPS and ICP-OES analyses reveal a metal (Na, Ni, Co, and Mn) content of about 0.4% and less than 0.7%, respectively, underlining the high purity of the recycled graphite. The carbon (96.3%) and oxygen (3.2%) contents determined by XPS are, in fact, comparable to the values obtained for commercial graphite.²⁰ In line with this, the XRD pattern recorded for the recycled graphite is in perfect agreement with the PDF reference for graphite and does not show any additional phases (Figure 2E). Similarly, the Raman spectrum (Figure 2F) presents the characteristic graphite features, that is, the graphitic G band at 1577 cm^{-1} ,²¹ the D band at 1350 cm^{-1} , indicating some disorder in the graphite lattice,^{22,23} and the overtone-derived D* bands at 2450 and 2713 cm^{-1} as well as the G* band at 3240 cm^{-1} .²⁴ The ratio of the intensity (I) of the D and G band (i.e., I_D/I_G) is about 0.41, which indicates a high degree of graphitic ordering, comparable to commercial graphite (Figure S3).^{25,26}

3.3 | Electrochemical characterization in half-cells

In all half-cell experiments, the electrolyte used was 1 M LiPF_6 in a 1:1 volume mixture of EC and DEC, comprising moreover 2% of VC and 10% FEC. FEC was added to decrease the parasitic side reactions at the lithium-metal counter electrode.^{27,28} Figure 3A displays the cyclic voltammogram (CV) of the first sweep for the recycled graphite, and the subsequent nine sweeps are presented in Figure 3B, revealing high reversibility. The CV profiles show the characteristic features of the de-/lithiation process with two reduction peaks at about 0.19 V and between 0.07 and 0.01 V versus Li^+/Li for the Li^+ intercalation and two oxidation peaks at around 0.15 and 0.24 V versus Li/Li^+ for the subsequent

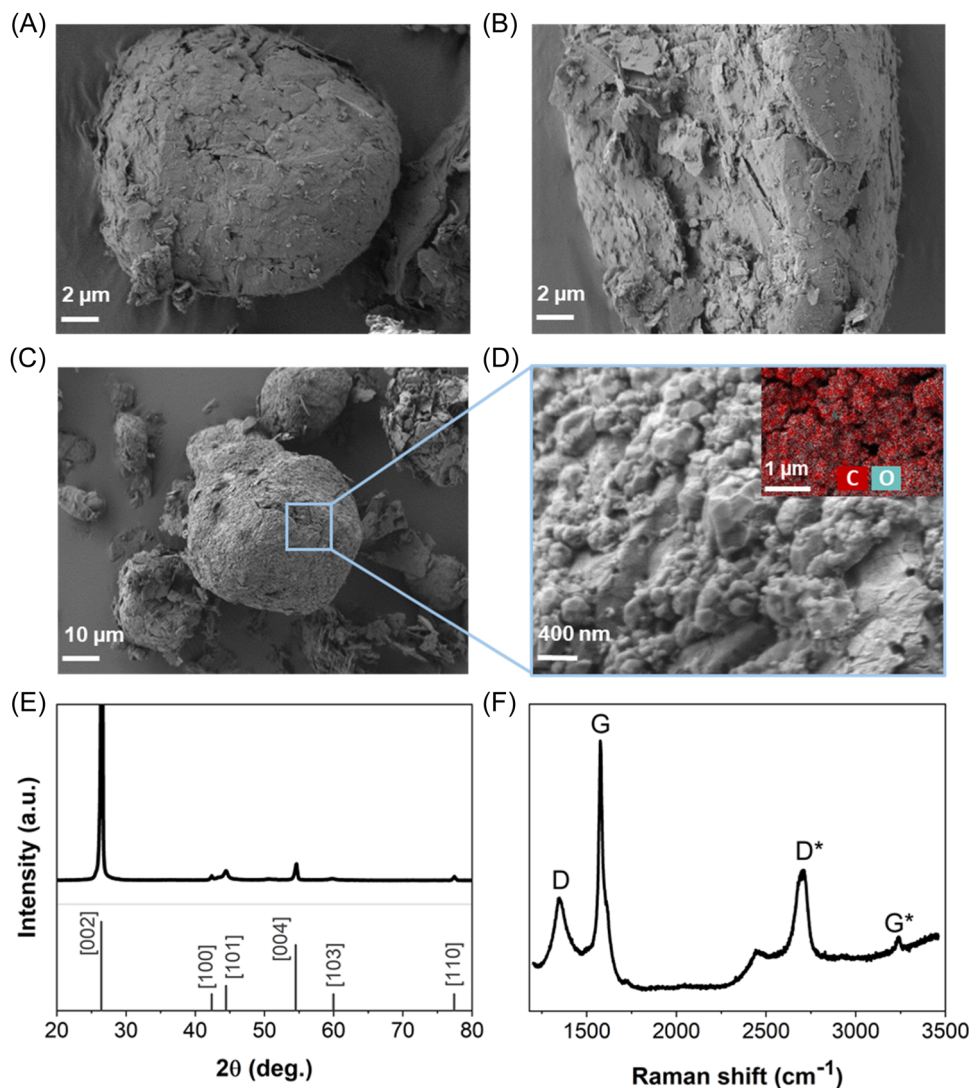


FIGURE 2 Physicochemical characterization of recycled graphite: (A–C) SEM images of different particles and at varying magnification; (D) close-up of the indicated area in (C), highlighting the surface morphology with an EDX mapping of carbon (in red) and oxygen (in light turquoise) as inset; (E) XRD pattern with the PDF reference no. 00-008-0415 (space group: $P6_3/mmc$) for graphite in the bottom; (F) Raman spectrum with an indication of the different bands observed.

deintercalation.^{29,30} Similarly, the galvanostatic discharge and charge profile of the first cycle in Figure 3C shows the expected well-defined voltage plateaus as the typical signature of the stage transitions that occur during the de-/lithiation of graphite.³⁰ The galvanostatic first cycle, moreover, reveals a reversible specific capacity of 351 mAh g^{-1} at C/20, along with a remarkable initial Coulombic efficiency (ICE) of 85.9%. This value is very reproducible, as confirmed by the additional cells tested (see Figure S4A), and is comparable to that of commercial graphite materials.^{26,31} The continuous cycling at 1 C for 200 cycles (Figure 3D) confirms that these electrodes own high cycling stability with a capacity retention of 95% when comparing the 13th cycle (i.e., the first cycle at 1 C after several formation cycles; 338 mAh g^{-1}) and the

212th cycle (321 mAh g^{-1}). Overall, the performance metrics of recycled graphite are comparable to those obtained with a pristine commercial graphite with a similar particle morphology (see the Supporting Information for further details), which provides an ICE of 87.4%, a reversible capacity of about 356 mAh g^{-1} at 1 C, and a capacity retention of about 98% after 200 cycles at 1 C (see Figure S4C,D).

3.4 | Evaluation in graphite||NMC₅₃₂ full cells

The suitability of the recycled graphite as a high-performance anode active material was eventually studied

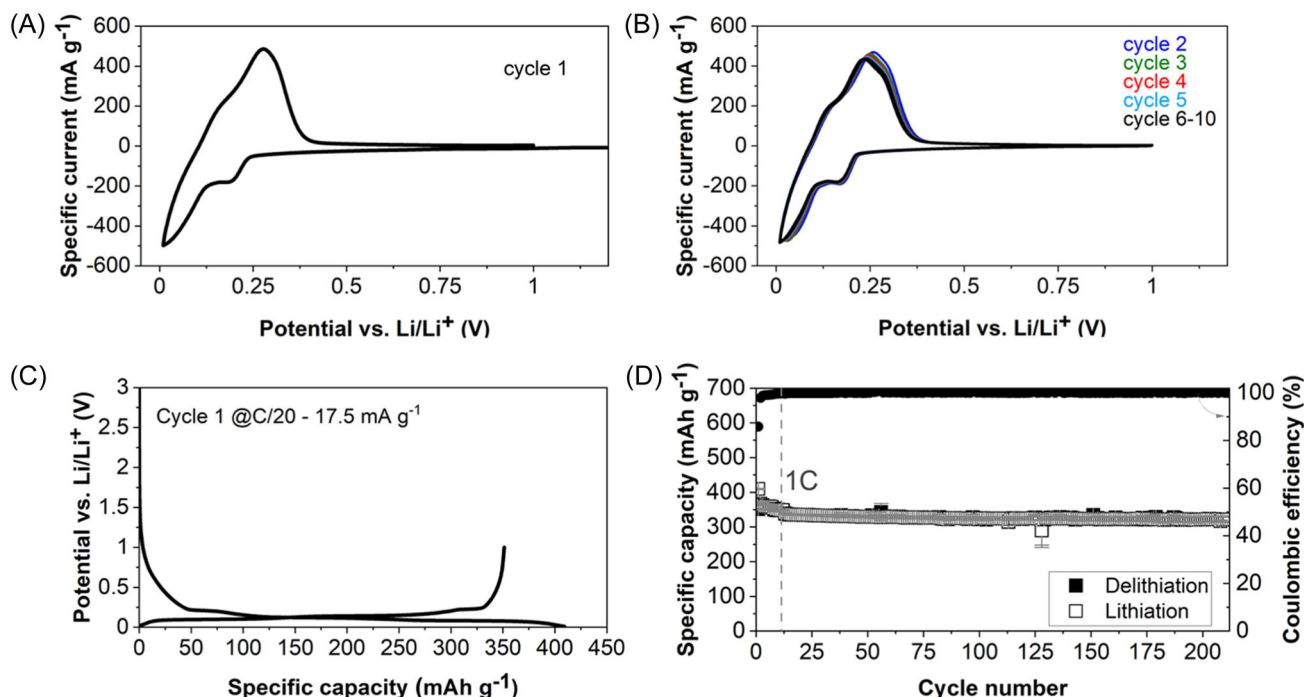


FIGURE 3 Electrochemical characterization of recycled graphite electrodes in half-cells with lithium-metal counter and reference electrodes: (A) Cyclic voltammogram of the first cyclic sweep and (B) the subsequent nine cyclic sweeps at a sweep rate of 0.1 mV s^{-1} (reversing potentials: 0.01 and 1.0 V vs. Li^+/Li). (C) First cycle galvanostatic discharge/charge profile at C/20, equivalent to a specific current of 17.5 mA g^{-1} , applying the same cutoff potentials. (D) Plot of the specific capacity and CE versus cycle number—the first cycle was conducted at C/20, the second at C/10, the next five cycles at C/5, and additional five cycles at C/2, before increasing the C rate to 1 C for another 200 cycles (the average of three cells is shown along with the standard deviation represented by the error bars).

in lithium-ion cells comprising $\text{Li}[\text{Ni}_{0.5}\text{Mn}_{0.3}\text{Co}_{0.2}]\text{O}_2$ (NMC_{532}) as the active material for the cathode. The electrodes were balanced to an anode/cathode capacity (N:P) ratio of 1.10, using their experimentally determined capacities at C/20. In the first step, we used the same electrolyte as for the half-cell tests (i.e., 1 M LiPF_6 in EC:DEC (1:1 by vol/vol) + 2% VC + 10% FEC) and performed a comparison with lithium-ion cells comprising the same cathodes, but SLP30 as commercially available graphite. The results are presented in Figure 4 and show that the cells employing recycled and pristine graphite provide a very comparable cycling performance and capacity retention for more than 600 cycles, thus further highlighting the excellent performance of recycled graphite. Generally, though, the capacity retention reached the limit of 80% rather early for both cells, which we assigned to a non-ideal electrolyte composition for such cell chemistry. Accordingly, we modified the electrolyte composition eliminating FEC in the subsequent experiments (i.e., we used 1 M LiPF_6 in EC:DMC (1:1) vol/vol + 2% VC as the electrolyte for all the forthcoming experiments). Figure 5A–D shows graphite|| NMC_{532} full-cell tests with recycled graphite conducted in three-electrode cells with a lithium-metal reference electrode. This setup allows for deconvoluting the behavior of the anode (in black) and cathode (in red) in the full cell

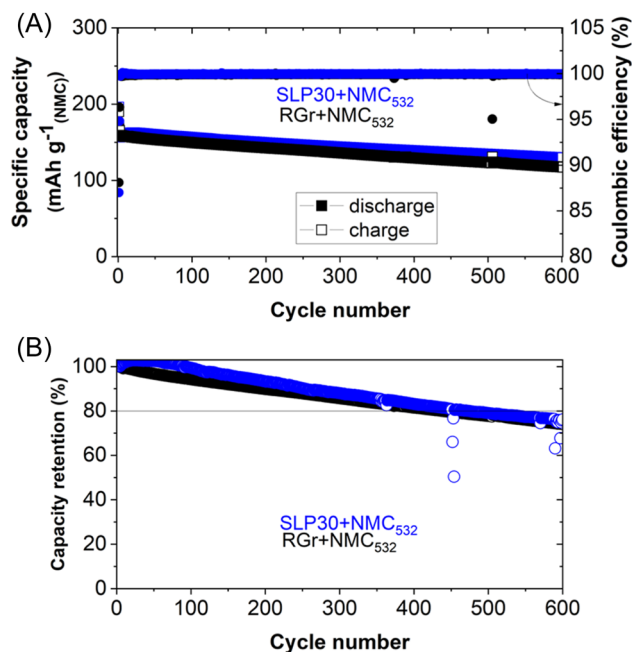


FIGURE 4 Comparison of the cycling performance of lithium-ion cells comprising NMC_{532} for the cathode and the recycled graphite (in black) and SLP30 (in blue) for the anode: (A) plot of the specific capacity referring to the NMC_{532} cathode and CE as a function of cycle number (first cycle at C/20, subsequent cycles at C/2). (B) Plot of the corresponding capacity retention as a function of cycle number.

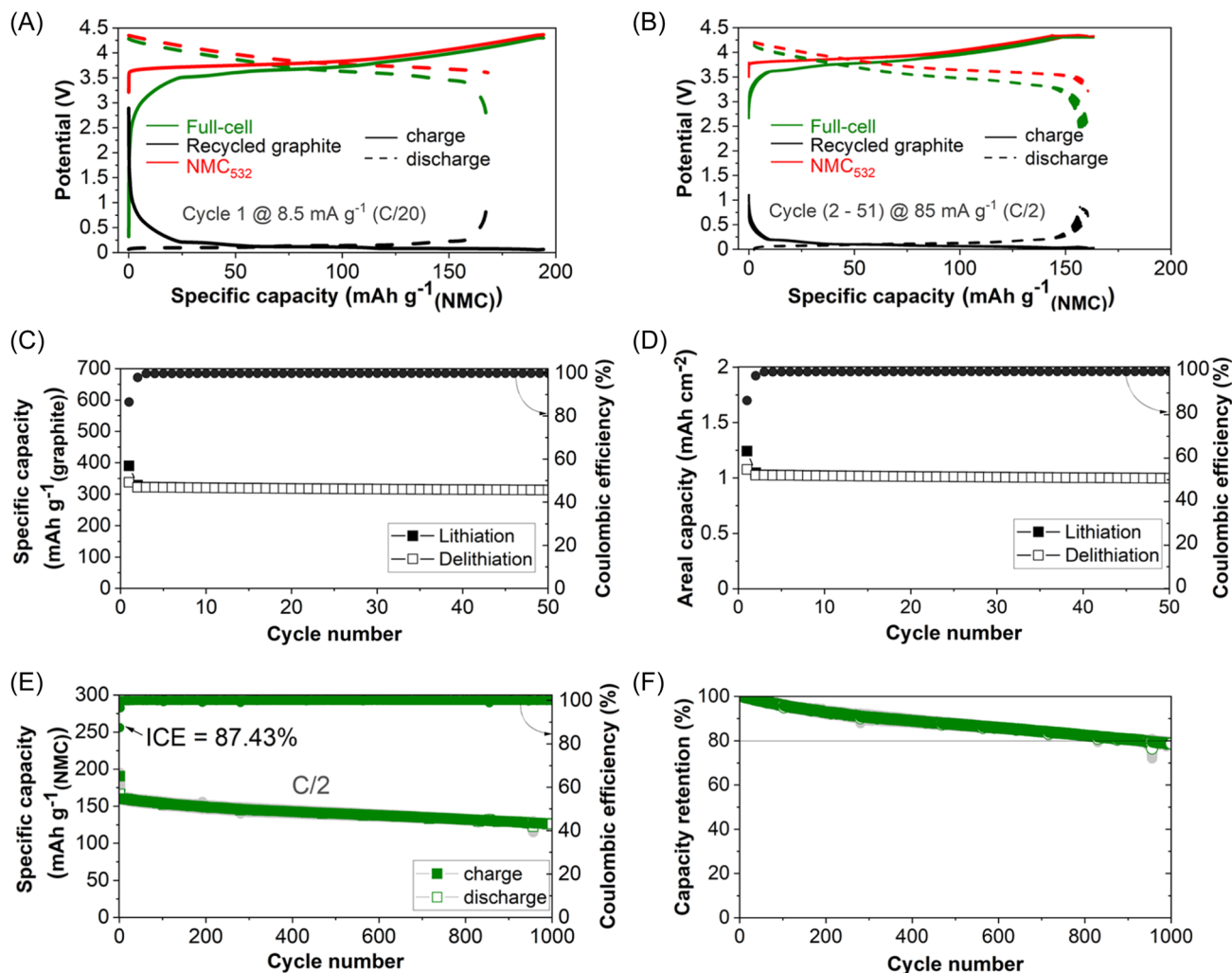


FIGURE 5 Electrochemical characterization of graphite||NMC₅₃₂ full cells in (A–D) three-electrode and (E, F) two-electrode cells: (A) Deconvolution of the first cycle charge (solid lines) and discharge (dashed lines) profiles of the graphite anode (in black) and the NMC₅₃₂ cathode (in green) from the full-cell profile (in red)—the first cycle was conducted at a specific current of 8.5 mA g⁻¹ (C/20 with regard to the cathode). (B) Evolution of the different discharge/charge profiles in the subsequent 50 cycles at C/2 with an indication of the changes occurring. (C) Plot of the specific capacity (referring to the mass of the graphite anode) and CE as a function of the cycle number. (D) The corresponding plot of the areal capacity. (E) Plot of the average specific capacity (referring to the NMC₅₃₂ cathode) and CE of the two-electrode graphite||NMC₅₃₂ full cells. (F) Plot of the corresponding average capacity retention at C/2 with an indication of the 80% limit (the standard deviation, indicated by the error bars, is negligible, i.e., hardly detectable).

(in green). The first charge capacity was 194 mA h g⁻¹ (referring to the mass of NMC₅₃₂ in the cathode) and the subsequent discharge capacity was 168 mA h g⁻¹, resulting in an ICE of 86.6% at C/20 (Figure 5A). In the subsequent 50 cycles conducted at C/2, this process is highly reversible and the capacity remains very stable, as displayed in Figure 5B–D. Nonetheless, a closer inspection of Figure 5B also reveals that there is a slight capacity fading upon cycling and that this essentially results from a shortening of the galvanostatic NMC₅₃₂ charge profile, accompanied by minor increase in capacity obtained during the subsequent constant voltage step at the upper cutoff potential. Simultaneously, the lower cutoff of the cathode

is increasing, while the upper cutoff of the anode is slightly increasing, indicating that there is a loss of electrochemically active lithium in the system, presumably owing to side reactions at the electrode–electrolyte interfaces. However, the plot of the specific capacity referring to the mass of graphite (Figure 5C) shows that this capacity loss is very minor and that the areal capacity of the graphite electrode (and accordingly also of the NMC₅₃₂ cathode) always remains above 1 mA h cm⁻² (Figure 5D), which is a reasonable value for lab-scale experiments. In fact, it should also be considered that the lithium-metal reference electrode may partly react with the electrolyte, introducing decomposition products that

affect the cell performance. Hence, extended cycling tests in two-electrode coin cells were also performed. Three full cells were evaluated, showing excellent reproducibility (Figure S5), and the average values along with the standard deviation are plotted in Figure 5E,F. The average ICE was 87.4%, that is, slightly higher than that in the three-electrode setup, which might be related to the absence of the lithium-metal reference electrode, and the average Coulombic efficiency (CE) was 99.95%. As a result, the two-electrode graphite||NMC₅₃₂ provided remarkable cycling stability (Figure 5E) and capacity retention of 80% after about 1000 cycles (precisely, around 950 cycles; Figure 5F), confirming that the recycled graphite is a highly suitable active material for the assembly of new high-performance lithium-ion cells. To further corroborate the suitability of recycled graphite as a potential alternative for high-performance LIBs, we doubled the active material mass loading to yield an areal capacity of about 2 mAh cm⁻² and evaluated these as well in graphite||NMC₅₃₂ full cells (Figure S6). Also, these cells showed a suitable ICE of about 88.0% (i.e., even slightly higher than that the cells comprising the 1 mAh cm⁻² electrodes), an average CE of 99.99%, and a capacity retention of about 80% after 1000 cycles.

4 | CONCLUSION

The successful use of recycled graphite obtained via a highly efficient froth-flotation method as anode material for LIBs has been demonstrated—to the best of our knowledge for the first time. The physicochemical characterization revealed only very minor metallic impurities with no significant impact on the material performance—neither in half-cells nor in graphite||NMC₅₃₂ full cells, allowing for an excellent cycling stability of the latter for more than 1000 cycles with a capacity retention of about 80%. In fact, the performance of recycled graphite in full cells is comparable to that of pristine commercial graphite, underlining the great potential of this recycling process and the potential direct recovery of graphite for the production of more sustainable LIBs.

ACKNOWLEDGMENTS

Mayokun Olutogun, Dominic Bresser, and Stefano Passerini would like to thank the Federal Ministry of Education and Research (BMBF) for financial support within the HighSafe project (03XP0138C) and the HighSafe-2 project (03XP0306C). Moreover, the authors would like to acknowledge financial support from the Helmholtz Association. Anna Vanderbruggen and Martin Rudolph acknowledge the Helmholtz-Institut Freiberg für Ressourcentechnologie for base funding within the PoF III (project-oriented funding part III) in

the frame of the BooMeRanG project. Moreover, the authors would like to acknowledge the Accurec GmbH for providing the black mass and UVR FIA GmbH for the help with sample splitting and the XRF analysis. Open Access funding enabled and organized by Projekt DEAL

CONFLICT OF INTEREST STATEMENT

The authors declare that there are no conflicts of interests.

DATA AVAILABILITY STATEMENT

The data generated during the current study are available from the corresponding authors upon reasonable request.

ORCID

Mayokun Olutogun  <http://orcid.org/0000-0001-5711-3418>

Anna Vanderbruggen  <http://orcid.org/0000-0003-4092-4374>

Martin Rudolph  <http://orcid.org/0000-0002-5374-6135>

Dominic Bresser  <http://orcid.org/0000-0001-6429-6048>

Stefano Passerini  <http://orcid.org/0000-0002-6606-5304>

REFERENCES

- Li M, Lu J, Chen Z, Amine K. 30 Years of lithium-ion batteries. *Adv Mater*. 2018;30(33):1800561.
- Marinaro M, Bresser D, Beyer E, et al. Bringing forward the development of battery cells for automotive applications: perspective of R&D activities in China, Japan, the EU and the USA. *J Power Sources*. 2020;459:228073.
- Armand M, Axmann P, Bresser D, et al. Lithium-ion batteries—current state of the art and anticipated developments. *J Power Sources*. 2020;479:228708.
- Bai Y, Muralidharan N, Sun YK, Passerini S, Stanley Whittingham M, Belharouak I. Energy and environmental aspects in recycling lithium-ion batteries: concept of battery identity global passport. *Mater Today*. 2020;41:304-315.
- Velázquez-Martínez O, Valio J, Santasalo-Aarnio A, Reuter M, Serna-Guerrero R. A critical review of lithium-ion battery recycling processes from a circular economy perspective. *Batteries*. 2019;5(4):68.
- Werner D, Peuker UA, Mütze T. Recycling chain for spent lithium-ion batteries. *Metals*. 2020;10(3):316.
- Porvali A, Aaltonen M, Ojanen S, et al. Mechanical and hydrometallurgical processes in HCl media for the recycling of valuable metals from Li-ion battery waste. *Resour Conserv Recycl*. 2019;142:257-266.
- Vanderbruggen A, Hayagan N, Bachmann K, et al. Lithium-ion battery recycling—influence of recycling processes on component liberation and flotation separation efficiency. *ACS ES&T Eng*. 2022;2(11):2130-2141.
- Salces AM, Bremerstein I, Rudolph M, Vanderbruggen A. Joint recovery of graphite and lithium metal oxides from spent lithium-ion batteries using froth flotation and investigation on process water re-use. *Miner Eng*. 2022;184:107670.
- Kim Y, Matsuda M, Shibayama A, Fujita T. Recovery of LiCoO₂ from wasted lithium ion batteries by using mineral processing technology. *Resour Process*. 2004;51(1):3-7.

11. Traore N, Kelebek S. Characteristics of spent lithium ion batteries and their recycling potential using flotation separation: a review. *Miner Process Extr Metall Rev.* 2022;44(3): 231-259.
12. Zhan R, Yang Z, Bloom I, Pan L. Significance of a solid electrolyte interphase on separation of anode and cathode materials from spent Li-ion batteries by froth flotation. *ACS Sustainable Chem Eng.* 2021;9(1):531-540.
13. Vanderbruggen A, Sygusch J, Rudolph M, Serna-Guerrero R. A contribution to understanding the flotation behavior of lithium metal oxides and spheroidized graphite for lithium-ion battery recycling. *Colloids Surf A.* 2021;626:127111.
14. Ruismäki R, Rinne T, Dańczak A, Taskinen P, Serna-Guerrero R, Jokilaakso A. Integrating flotation and pyrometallurgy for recovering graphite and valuable metals from battery scrap. *Metals.* 2020;10(5):680.
15. European Parliament. EU Legislation in progress: new EU regulatory framework for batteries setting sustainability requirements. 2021.
16. Asenbauer J, Eisenmann T, Kuenzel M, Kazzazi A, Chen Z, Bresser D. The success story of graphite as a lithium-ion anode material—fundamentals, remaining challenges, and recent developments including silicon (oxide) composites. *Sustainable Energy Fuels.* 2020;4(11):5387-5416.
17. European Commission. Critical raw materials resilience: charting a path towards greater security and sustainability. 2020.
18. Vanderbruggen A, Salces A, Ferreira A, Rudolph M, Serna-Guerrero R. Improving separation efficiency in end-of-life lithium-ion batteries flotation using attrition pre-treatment. *Minerals.* 2022;12(1):72.
19. Vanderbruggen A, Gugala E, Blannin R, Bachmann K, Serna-Guerrero R, Rudolph M. Automated mineralogy as a novel approach for the compositional and textural characterization of spent lithium-ion batteries. *Miner Eng.* 2021;169:106924.
20. Blyth RIR, Buqa H, Netzer FP, et al. XPS studies of graphite electrode materials for lithium ion batteries. *Appl Surf Sci.* 2000;167(1-2):99-106.
21. Tuinstra F, Koenig JL. Raman spectrum of graphite. *J Chem Phys.* 1970;53(3):1126-1130.
22. Ferrari AC, Robertson J. Interpretation of Raman spectra of disordered and amorphous carbon. *Phys Rev B.* 2000;61(20): 14095-14107.
23. Pimenta MA, Dresselhaus G, Dresselhaus MS, Cançado LG, Jorio A, Saito R. Studying disorder in graphite-based systems by Raman spectroscopy. *Phys Chem Chem Phys.* 2007;9(11): 1276-1290.
24. Nemanich RJ, Solin SA. First- and second-order Raman scattering from finite-size crystals of graphite. *Phys Rev B.* 1979;20(2):392-401.
25. Foss CEL, Svensson AM, Sunde S, Vullum-Bruer F. Edge/basal/defect ratios in graphite and their influence on the thermal stability of lithium ion batteries. *J Power Sources.* 2016;317:177-183.
26. Placke T, Siozios V, Schmitz R, et al. Influence of graphite surface modifications on the ratio of basal plane to “non-basal plane” surface area and on the anode performance in lithium ion batteries. *J Power Sources.* 2012;200:83-91.
27. Markevich E, Salitra G, Aurbach D. Fluoroethylene carbonate as an important component for the formation of an effective solid electrolyte interphase on anodes and cathodes for advanced Li-ion batteries. *ACS Energy Lett.* 2017;2(6): 1337-1345.
28. Zhang XQ, Cheng XB, Chen X, Yan C, Zhang Q. Fluoroethylene carbonate additives to render uniform Li deposits in lithium metal batteries. *Adv Funct Mater.* 2017;27(10): 1605989.
29. Dahn JR. Phase diagram of Li_xC_6 . *Phys Rev B.* 1991;44(17): 9170-9177.
30. Heß M, Novák P. Shrinking annuli mechanism and stage-dependent rate capability of thin-layer graphite electrodes for lithium-ion batteries. *Electrochim Acta.* 2013;106:149-158.
31. Sivakkumar SR, Nerkar JY, Pandolfo AG. Rate capability of graphite materials as negative electrodes in lithium-ion capacitors. *Electrochim Acta.* 2010;55(9):3330-3335.

SUPPORTING INFORMATION

Additional supporting information can be found online in the Supporting Information section at the end of this article.

How to cite this article: Olutogun M, Vanderbruggen A, Frey C, Rudolph M, Bresser D, Passerini S. Recycled graphite for more sustainable lithium-ion batteries. *Carbon Energy.* 2024;e483. doi:10.1002/cey2.483